Contrib Mineral Petrol (2016) 171:75
DOI 10.1007/s00410-016-1286-0

ORIGINAL PAPER

Hydrous albite magmas at lower crustal pressure: new results on liquidus H_2O content, solubility, and H_2O activity in the system $NaAlSi_3O_8$–H_2O–NaCl at 1.0 GPa

A. R. Makhluf[1] · R. C. Newton[1] · C. E. Manning[1]

Received: 29 April 2016 / Accepted: 2 August 2016 / Published online: 18 August 2016

Abstract The system albite–H_2O serves as an important model for the generation of granitic magmas, yet relatively few experimental investigations have focused on phase relations at high pressure. This study reports new experimental results, at 1.0 GPa and 690–1050 °C, on the temperature and liquid composition at vapor-saturated melting, the H_2O content of undersaturated silicate liquids in equilibrium with albite, the solubility of albite in H_2O–NaCl fluids immediately below the solidus, and the activity of H_2O in hydrous $NaAlSi_3O_8$ liquids along the liquidus. Albite melts and dissolves congruently at all temperatures and salinities. In the NaCl-absent system, the temperature of vapor-saturated melting of low albite, confirmed by X-ray diffraction, is 695 ± 5 °C and the liquid composition is 18.14 ± 1.35 wt% H_2O. The temperature dependence of the fluid-undersaturated liquidus curve in the system $NaAlSi_3O_8$–H_2O varies with H_2O wt% (w_{H_2O}) according to

$$T = -2.0331 \times 10^{-3} w_{H_2O}^3 + 1.6497 w_{H_2O}^2 - 58.963 w_{H_2O} + 1235.5\,^{\circ}C$$

indicating positive curvature in temperature-composition coordinates and a dry melting temperature of ~1235 °C. At 690 °C, immediately below the solidus, albite solubility decreases drastically with NaCl content of the fluid phase, from 8.8 ± 0.6 wt% in the NaCl-free fluid to ˂2 % at NaCl concentration of only 10 mol%. Experiments determining the activity of H_2O (a_{H_2O}) in liquids at vapor-saturated melting exploited low Cl solubility in liquids and low albite solubility in the presence of H_2O–NaCl fluids. The maximum Cl content of quenched glasses, only 0.95 wt%, and very low albite solubility together make possible H_2O activity measurement in melts equilibrated with NaCl–H_2O solutions. When combined with activity data for H_2O–NaCl fluids, experimentally determined a_{H_2O} along the liquidus is described by

$$T = -469.16 a_{H_2O}^{L\,\frac{1}{2}} - 93.382 a_{H_2O}^{L} + 1235.5\,^{\circ}C.$$

At 1 GPa, H_2O activities in hydrous albitic melts in H_2O–NaCl fluids agree with those in the presence of H_2O–CO_2 fluids, provided appropriate fluid mixing data are used. Our results constrain an asymmetric regular solution model for the mixing of $Na_{1/8}Al_{1/8}Si_{3/8}O$ and H_2O, yielding Margules parameters of W_{Ab} = 25.56 ± 0.54 and W_{H_2O} = 10.50 ± 0.74 kJ/mol. The results imply critical mixing of liquid and vapor at ~1100 °C. Using existing speciation models, our results imply that H_2O dissolved in hydrous albitic liquids is almost entirely in the form of molecular H_2O (OH^- concentration is negligible) at temperatures near vapor-saturated melting. The results provide a more complete experimental foundation for modeling the system $NaAlSi_3O_8$–H_2O at high pressure.

Keywords Activity · Albite · Liquidus · Solubility · Speciation · Brine · Solvus · Miscibility · Granite · Magma · Margules · Supercritical fluid · Critical phenomena

Communicated by Mark S Ghiorso.

✉ A. R. Makhluf
amakhluf@epss.ucla.edu

[1] Department of Earth, Planetary and Space Sciences, University of California, Los Angeles, Los Angeles, CA, USA

Introduction

The fundamental importance of H_2O in the origin of granitic magma was first shown by Goranson (1938). His melting experiments on albite ($NaAlSi_3O_8$) at elevated H_2O pressures revealed a dramatic decrease of the melting temperature from above 1100 °C to 800 °C at 0.4 GPa. Subsequently, the pressure dependence of the H_2O-saturated melting point of albite was more fully characterized, and the greatest decrease in melting temperature was shown to be near 630 °C at 1.7 GPa, where the breakdown of albite to jadeite ($NaAlSi_2O_6$) plus quartz reverses the melting trend (Boettcher and Wyllie 1969).

Because alkali feldspar is the dominant mineral component of granite, the simple system $NaAlSi_3O_8$–H_2O serves as a useful model for understanding melting in the earth's crust. Further refinements in melting experiments included $KAlSi_3O_8$ and quartz under H_2O-saturated conditions (Tuttle and Bowen 1958; Luth et al. 1964). Their experiments showed that if H_2O is sufficiently abundant in deep-crustal processes, H_2O-rich granites can form in the temperature range thought to prevail in high-grade metamorphism, leading to the concept of anatexis as "ultra-metamorphism" (Brown and Fyfe 1970).

Another illustration of the important role of H_2O in deep-crustal processes was the demonstration by Shen and Keppler (1997) of critical mixing of liquid and vapor in the system $NaAlSi_3O_8$–H_2O. They showed, by direct observation in an externally heated diamond pressure cell, that H_2O-rich albitic liquids and $NaAlSi_3O_8$-rich aqueous fluids are miscible in all proportions at pressures in the deep-crustal range and temperatures of high-grade metamorphism (1.0–1.5 GPa and 700–1000 °C). The possibility exists of supercritical or near-critical hydrous silicate magmas as important agents of deep-crustal and upper mantle metasomatism and differentiation.

A comprehensive understanding of the system $NaAlSi_3O_8$–H_2O at elevated pressures has been inhibited by lack of adequate phase composition data, principally of H_2O solubility in silicate melts and the solubility of albite and silicate melts in aqueous fluids. This has compromised analysis of the H_2O budget in magma genesis and prevented a phase equilibrium link between vapor-saturated melting and critical phenomena. Figure 1 illustrates outstanding problems with reference to the system $NaAlSi_3O_8$–H_2O. Most experimental determinations of melting at high pressure have focused on dry melting (Point A) or the vapor-saturated solidus (Point B). There have been numerous measurements of the H_2O concentration in the melt near B (see Silver and Stolper 1985 for a summary), but they display wide experimental scatter, chiefly due to problems of H_2O exsolution in quenching from high pressure (P) and temperature (T) and problems of calibration of

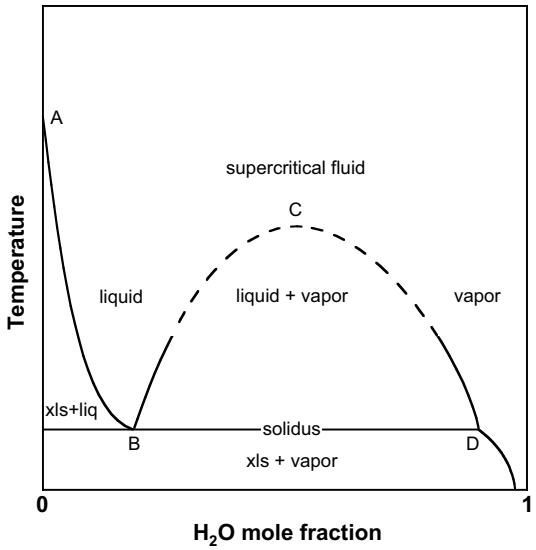

Fig. 1 Schematic isobaric phase relations of the system $NaAlSi_3O_8$–H_2O, projected onto the temperature-composition plane. A, dry melting point; B, H_2O-saturated melting point; C, crest of the liquid + vapor solvus; D, solubility of albite in H_2O at H_2O-saturated melting. The section portrays moderate to high pressures, where the maximum of the liquid + vapor loop can be expected to occur at intermediate compositions

the several methods used to analyze H_2O in the glass (drying weight loss, infrared spectroscopy, mass spectroscopy). Extrapolation of the determinations to the pressure range of deep-crustal melting and metamorphism ($0.5 \leq P \leq 1.5$ GPa) is accordingly uncertain.

Experimental determination of the H_2O content of fluid-undersaturated albitic liquids is even more uncertain. There have previously been no reversed measurements of liquidus compositions (Line A–B, Fig. 1). The main problem is difficulty in attaining equilibrium in unfluxed (fluid-absent) systems. Such data would be of considerable importance in evaluation of the H_2O budget in "dehydration melting" (Rutter and Wyllie 1988), where the only source of H_2O for melting is that resident in hydrous minerals such as micas.

The vapor-saturation curve (Line B–C, Fig. 1) is the link between hydrous melting, silicate solubility and possible critical mixing of silicate-rich liquid and H_2O-rich vapor (Point C). Most models of H_2O solubility do not anticipate critical phenomena, mainly because, in order to avoid H_2O exsolution in quenched glasses, experimental measurements on which they are based were limited to small H_2O contents. Paillat et al. (1992) first recognized the possible existence of supercritical fluids at high pressures in the system $NaAlSi_3O_8$–H_2O based on improved ion-probe methods of analysis of rapidly quenched charges. They found that, at pressures greater than 0.4 GPa, H_2O solubility in albitic melts is prograde; that is, it increases with increasing temperature at constant pressure. This finding

contrasts with all previous results and implies that liquids may acquire enough H_2O to become supercritical mixtures with $NaAlSi_3O_8$, as is the case at about 1.0 GPa in the system SiO_2–H_2O (Kennedy et al. 1962; Newton and Manning 2008).

A critical point (Fig. 1, Point C) was located by Shen and Keppler (1997) at 1.0 GPa near 1100 °C and ~50 wt% H_2O. Their data prove very high H_2O solubility in silicate liquids. At the invariant temperature of the solidus, silicate solubility in aqueous fluids should still be substantial (Point D). This is a very important consideration—despite a few determinations of albite solubility in H_2O at high *P* and *T* (e.g., Burnham in Clark 1966; Anderson and Burnham 1983), and it has been common in thermodynamic models to neglect the composition of the vapor phase in equilibrium with the melt at the melting minimum. It can be shown that, in simple regular-solution type models, the critical temperature must approach infinity as the composition of the vapor phase tends to pure H_2O. Even in cases where albite solubility is explicitly taken into account (e.g., Zeng and Nekvasil 1996), inadequate knowledge of solubility contributes to inaccurate depiction of critical phenomena in the system. Therefore, an essential ingredient to any investigation aimed at quantitative characterization of phase relations across the full binary system is the determination of solubility of albite in H_2O.

A satisfactory model of hydrous melting should be consistent with measured thermodynamic data for minerals, melts and fluids, especially in attempted extrapolations beyond experimental *P*–*T* conditions. Many high-quality data exist for crystalline albite and $NaAlSi_3O_8$ glass, including heat capacities (Krupka et al. 1979; Stebbins et al. 1984), equation of state data for albite and glass (Lange and Carmichael, 1990; Benusa et al. 2005; Tribaudino et al. 2010) and *P*–*V*–*T* measurements on H_2O-bearing albitic melts (Burnham and Davis 1974). Additions of accurately determined binary melt compositions coexisting with albite or aqueous fluid over ranges of temperature and pressure would be an important complement to these data.

The present study was designed to provide some of the needed phase composition data in the system $NaAlSi_3O_8$–H_2O in a pressure–temperature region representative of melt generation in the deep crust (1.0 GPa and 690–1050 °C). The new measurements include liquidus H_2O contents (Line A–B, Fig. 1), liquid composition at the vapor-saturated solidus (Point B) and albite solubility in aqueous fluid at the vapor-saturated solidus (Point D). The vapor-absent liquidus compositions were determined by reversed liquid–crystal equilibration in order to eliminate the possibility of undercooling of liquid or superheating of crystals. Melt compositions at vapor saturation were investigated by textural analysis of quenched charges, by methods developed by Burnham and Jahns (1962). This method circumvents the problem of H_2O exsolution in quenched glasses that has plagued earlier investigations. The fast-quench capability of the piston-cylinder apparatus is an additional advantage—higher H_2O contents of glasses can be retrieved, in many cases, without bubble formation upon rapidly quenching. The solubility of a pure natural albite was measured at temperature near the solidus, by single-crystal weight loss and by noting incipient crystal saturation in solutions with progressively greater $NaAlSi_3O_8$ content. These methods were developed to measure solubilities of many different minerals at high temperatures and pressures (Newton and Manning 2010; Manning and Aranovich 2014). In the course of the new experiments, we found that solute NaCl greatly inhibits albite solubility at high pressure and that the Cl partitioning into coexisting albitic melts is very small. These features make possible measurement of H_2O activity in the melts, since H_2O activity in NaCl solutions has been determined over large ranges of temperature, pressure and composition (Aranovich and Newton 1996). The measured H_2O activity data are used to calibrate a thermodynamic framework that links H_2O-undersaturated melts to vapor-saturated melts and supercritical fluids. This model is, in turn, useful in evaluating H_2O speciation in H_2O-rich feldspathic melts, using theoretical models developed by previous workers.

Experimental and analytical methods

Analytical methods

The compositions and structural state of starting materials and run products were characterized by electron microprobe (EMP) analysis and powder X-ray diffraction (XRD). Electron microprobe analysis was conducted using a JEOL 8500 instrument. Operating conditions for the analysis of albite crystals were 15 kV, 15 nA and a 10-μm beam spot size. Counting times were 20 s on the sample and 5 s on the background for all elements except the alkali metals, which were measured for 10 s on the sample and 5 s on the background. The standards used were a Tiburon albite (for Si, Al and Na), a St. Gotthard, Switzerland adularia (for K), a Great Sitkin Island, Alaska anorthite (for Ca) and a Minas Gerais, Brazil magnetite (for Fe). For analysis of hydrous glasses, the beam was defocused to 14 μm and the current lowered to 6 nA to minimize H and Na loss. The counting time was 20 s on the sample and 5 s on the background. The same standards were used, but in addition Cl was analyzed using a PETH crystal and a synthetic barium chlorapatite standard provided by the University of Michigan.

We employed powder XRD to characterize run products and determine unit cell constants of starting and run-product albite. A PANalytic powder diffractometer

and Cu Kα ($\lambda = 1.5408$ Å) radiation were used. Scans to check for the presence or absence of albite were conducted at $20° < 2\theta < 60°$ at ~2° 2θ min^{-1}. Scans to assess albite structural state were carried out at $28° \leq 2\theta \leq 32°$ at ½° 2θ min^{-1}. The (111) peak from a high purity silicon wafer at 28.440° 2θ was used to calibrate and index the diffraction peaks. We then calculated the 2θ difference between the 131 and $1\bar{3}1$ peaks ($\Delta 2\theta_{131-1\bar{3}1}$) to characterize the albite structural state.

Starting materials

Starting materials were a well-characterized natural low albite from Amelia County Court House (Virginia, USA), ultrapure water (~18 MΩ cm^2/cm resistivity) and reagent grade Fischer Scientific NaCl.

The largest impurities in the albite were <0.20 wt% K_2O and <0.20 wt% CaO. The $\Delta 2\theta_{131-1\bar{3}1} = 1.076°$ in the starting albite indicates the low structural state and is consistent with results of Newton and Smith (1967). Knowledge of the structural state of the albite starting material is important because the liquidus melting relationships will change depending on structural state (Goldsmith and Jenkins 1985a, b).

Finely ground albite was used for all experiments except for single-crystal weight loss solubility experiments in H_2O–NaCl solutions. The albite was ground under acetone in an agate mortar for ~30 min until complete evaporation and then dried in an oven at 600 °C for ~30 min to volatilize any organic residue.

Platinum tubing segments of ~1.25–1.75 cm length and 2.0 or 3.5 mm diameter were used for the experiments. The tubing segments were cleaned with acetone; then one side of each of the capsules was sealed with an oxy-acetylene flame and the whole capsule annealed.

Water mole fractions ranged from 0.035 to 0.99. The dry charge was weighed into a capsule, and then the H_2O was added with a microliter syringe. A mass of H_2O slightly larger than the target value was added and allowed to evaporate on the balance until the desired weight was reached. The capsule was then pinched and sealed by arc welding. Weight loss on sealing was typically less than 50 μg, all of which is attributable to platinum evaporation. The amounts of total charge ranged from ~10 to 60 mg. Weighing was carried out on a Mettler-Toledo UMX2 ultra-microbalance with a stated precision of 2×10^{-4} mg. Multiple weighings were made after adding each component to the capsules, and weighing errors were propagated to calculate uncertainties in concentrations and activities. Capsules were weighed before and after all runs to ensure that no water was lost during the experiment. Any experiments that lost more than ~15 μg during the course of the experiment were discarded. It is important to note that the ability to seal accurately weighed amounts of H_2O without appreciable weight loss and to demonstrate that no loss occurs during an experiment at high P and T, is essential to accurate characterization of the key phase boundaries in Fig. 1.

Piston-cylinder methods

Experiments were conducted in a piston-cylinder apparatus of either 2.54 or 1.91-cm diameter using NaCl-graphite furnace assemblies (Manning and Boettcher 1994; Newton and Manning 2000). Pressure measurements were made using Heise Co., bourdon tube gauges. Pressure uncertainties were ±0.03 GPa. Temperature was digitally measured and controlled to ±3°C using S-type thermocouples. An all-NaCl pressure medium was used at $T \leq 900$ °C (Manning and Boettcher 1994), but higher-temperature experiments required the use of small BN discs to prevent melting of the pressure medium in the vicinity of the capsule. The BN discs were 0.15 cm in length and placed immediately above and below the capsule. In addition, BN powder was packed around capsules in these high-temperature runs. The BN–NaCl pressure medium required a pressure correction of −0.06 GPa relative to the NaCl pressure medium, based on a comparison of quartz solubility in H_2O at 1.0 GPa, 950 °C, using an all-NaCl assembly (Manning 1994) with the BN–NaCl assembly.

Experiments were held at 1.0 GPa and desired temperature for 3–139 h. Run duration depended on the temperature and H_2O content. At the end of an experiment, runs were rapidly quenched to below 200 °C in ~30 s from temperatures between 690 and 1050 °C.

Interpretation of run products

Quenched charges were retrieved from opened capsules as glassy flat wafers in cases of substantial melting, or as loose, friable aggregates in the absence of melting. Phase relations involving albite (Ab), hydrous albitic liquid (L) and H_2O-rich fluid (also referred to as the vapor phase, V) were constrained by textural analysis of run products by binocular, petrographic and scanning electron microscopy (SEM). At 1.0 GPa, the experiments bracketed the liquidus curve at temperatures between the dry melting of albite and the $L + V$ miscibility gap at the vapor-saturated solidus. Criteria were developed to assign results to phase stability fields of Ab + V, Ab + L, L, and $L + V$ using a binocular microscope and/or immersion oil mounts and a petrographic microscope. In the albite–H_2O system, supersolidus conditions were indicated by the presence of glass in the run products. Dispersed, small, equant albite crystals, many rhomb-shaped, reflected recrystallization of starting albite. The run product seen in Fig. 2a was interpreted to indicate that run conditions corresponded to the Ab + L stability field. At a given temperature,

increasing the H_2O content yielded decreasing albite abundance in quenched charges. Run products characterized by the presence of a single homogeneous glassy phase and the absence of albite crystals were assigned to the liquid field. Experiments at vapor saturation ($L + V$) displayed evidence of two fluid phases in run products (Fig. 2b) and were consistent with textures observed by Burnham and Jahns (1962). The presence of a free vapor phase was indicated by pockets (void spaces) that usually formed at the interface between the capsule wall and the liquid, usually near the pinched ends of the capsule. The pockets at the top of the capsule are preserved during rapid quenching. Solutes dissolved in the vapor quench to small spheroidal balls of clear glass (Fig. 2b). As noted by Burnham and Jahns (1962), these features are evidence for the presence of a separate aqueous fluid phase coexisting with a silicate liquid.

Similar textural analysis methods were used to identify the run products from the experiments involving H_2O–NaCl fluids. Subsolidus charges were lightly sintered aggregates containing large (up to 100 μm) subhedral to euhedral albite crystals (Fig. 2c). Two experiments of comparatively short duration contained glassy slugs crowded with euhedral albite crystals (Fig. 2a), signaling incomplete reaction (see below). Completely melted charges at $T < 1000$ °C contained crystal-free, oblate glass spheroids (Fig. 2d), indicating $L + V$ coexistence. The small but nonnegligible amount of H_2O dissolved into the melt could be estimated by mass balance by weighing the glassy portion of the charge for a completely melted sample and subtracting the initial mass of albite weighed into the capsule. Since some H_2O exsolves from the albitic melt upon quenching, the amount of H_2O measured in the quenched glass by this procedure serves as a lower bound on the actual H_2O content that was in the melt. At 1000 °C and higher, some of the fully melted charges could not be removed intact, which prevented a determination of the H_2O depleted from the vapor phase.

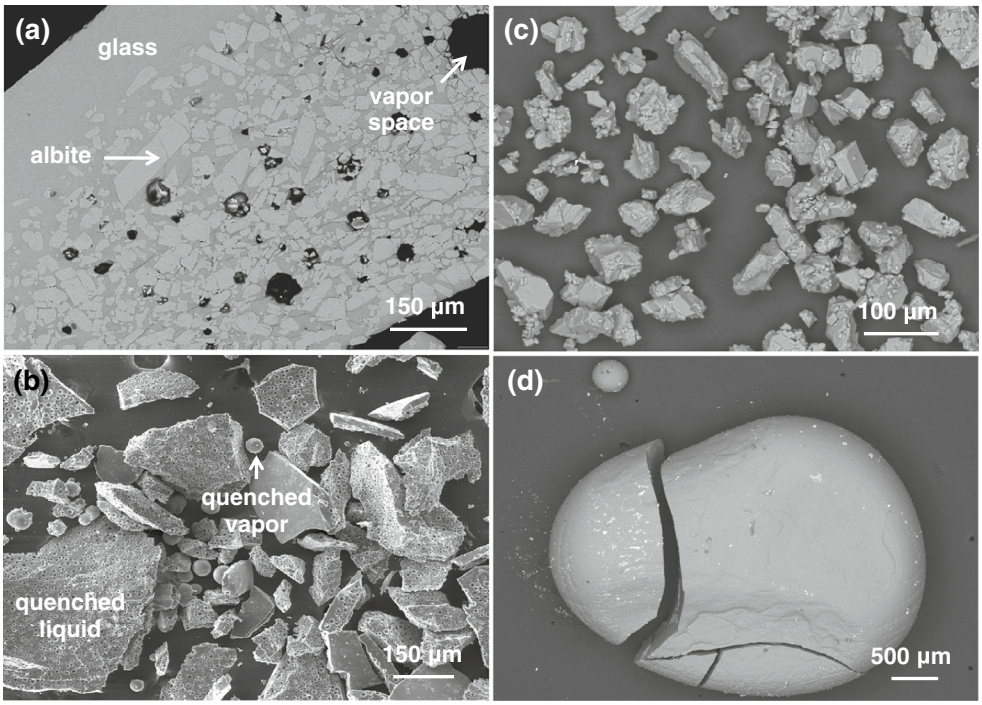

Fig. 2 Scanning electron photomicrographs of portions of quenched capsules and charges. **a** Backscattered electron image of textures in a run interpreted to be too short to yield complete melting. The partially melted charge contains segregated melt that formed at the top of the capsule, along with coarsely recrystallized, partially dissolved albite and possible vapor spaces. The vapor space contains halite crystals that formed during quench. Run Ab247, $P = 1.0$ GPa, $T = 950$ °C, with NaCl, $a_{H_2O} = 0.297$. **b** Secondary electron image of a quenched charge showing evidence for equilibrium between liquid and a coexisting vapor phase at experimental conditions. Hydrous albite liquid quenches to a bubbly glass from which minor H_2O has exsolved. A fluid appears in equilibrium with the liquid phase as evidenced by clear glass balls that formed in the quench from a former vapor space. Run Ab27, $P = 1.0$ GPa, $T = 800$ °C, with 26.13 wt % H_2O, no NaCl. **c** Backscattered electron image of an unmelted charge in which albite coexisted with H_2O–NaCl fluid. Quench halite was dissolved away with water, leaving behind recrystallized euhedral crystals of albite. Run Ab248, $P = 1.0$ GPa, $T = 950$ °C, with NaCl, $a_{H_2O} = 0.259$. **d** Backscattered electron image showing a quenched melt spheroid quenched from melt typically observed in crystal-free H_2O–NaCl liquidus experiments. High intensity (*white*) specks on the glass spheroid are halite crystals. Run Ab250, $P = 1.0$ GPa, $T = 950$ °C, with NaCl, $a_{H_2O} = 0.311$

Solubility measurements

The solubility of albite in $H_2O \pm NaCl$ was determined in order to constrain the isobaric-invariant composition of the H_2O-rich limb of the solvus at the solidus and its variation with H_2O activity. All experiments were conducted at 1.0 GPa and 690 °C, which is 10 °C lower than the lowest temperature at which melting was observed at this pressure.

Two types of solubility experiment were carried out. Ab_1 experiments yield a direct solubility determination, whereas Ab_2 experiments bracket solubility between upper and lower bounds by establishing the presence or absence of albite in quenched charges. The Ab_1 experiments determined albite solubility by measuring the weight loss of single crystals in NaCl-bearing fluids. All experiments were conducted at NaCl concentrations lower than halite saturation (Aranovich and Newton 1996). Crystals were hand picked so as to fit loosely into a 1.6-mm diameter platinum inner capsule. A weighed single crystal was loaded into the inner capsule and pinched lightly in order to allow H_2O fluid flow through the inner capsule. The inner capsule was burnished at both ends, punctured with four small holes of ~0.0025 cm diameter near the ends of the capsule and then weighed. The holes provided additional flow of fluid through the inner capsule. The inner capsule was loaded into the outer capsule, and NaCl was added, followed by ultrapure water. The outer capsule was then pinched and sealed by arc welding. After the experiment was run, the pH of quenched fluids was determined immediately upon puncturing of the outer capsule. The outer capsule was then opened with a razor blade and the inner capsule removed and soaked in warm water over a hot plate while stirring with a magnetic bar in order to remove quenched salt. The capsule was subsequently dried at 110 °C and weighed. This procedure was repeated up to five times until all of the halite was dissolved, as indicated by constant weight. The weight loss of the inner capsule after the experiment corresponds to the amount of albite dissolved in the solution, and thus the solubility of albite provided that dissolution is congruent. The absence of additional crystalline phases was established by optical and SEM inspection of opened inner capsules and albite surfaces.

Ab_2 experiments were required for runs in pure H_2O because of much higher albite solubility. This led to the formation of deep solution channels along fractures or cleavage planes of albite crystals, causing crystals to fragment into many small pieces, some of which could escape through the capsule perforations and lead to artificially high solubility. No inner capsule was used for these experiments, but instead finely ground albite was packed directly into a Pt capsule, H_2O was added, and the capsule was then pinched and sealed as done for the other experiments. Piston-cylinder methods were the same as for the other experiments. After opening, pH was measured with Hydrion® 1.0–12.0 pH paper. The capsules were then dried and inspected to establish the presence or absence of albite. Runs were also checked for the presence of additional phases. Using masses of albite and H_2O added to these runs, complete dissolution of albite gives a minimum solubility, whereas charges in which albite did not fully dissolve provide a maximum solubility.

Measurement of H_2O activity in albite liquids

H_2O activity at the liquidus was determined by bracketing the temperature of albite melting in the presence of fluids of known H_2O activity. Powdered low albite was equilibrated with a H_2O–NaCl solution of a given concentration. At equilibrium, the activity of H_2O in albite liquid is directly returned from the bracketed melting temperature because it must equal that in the coexisting vapor phase. We used the activity formulation of Aranovich and Newton (1996) and the H_2O equation of state of Holland and Powell (1991), which are applicable provided that there is negligible Cl in the melt and negligible albite solubility in the fluid (both of which were confirmed in the course of the study; see below). These experiments follow conceptually from previous work using H_2O–CO_2 fluids (e.g., Eggler and Kadik 1979; Bohlen et al. 1982), but exploit the very different activity–composition relations in H_2O–NaCl fluids (e.g., Manning and Aranovich 2014).

Experimental results

Equilibrium

We used several strategies to ensure and evaluate equilibrium. For the determination of the liquidus in the Ab–H_2O system, we employed long-run durations (19–93 h) to maximize the extent of reaction during runs bracketing phase boundaries. The liquidus brackets established in this manner were then checked by conducting selected reversal experiments. These were carried out in two steps. Initially, a charge with albite and H_2O was held at T well above the initially determined liquidus for time sufficient to completely melt the charge. The T was then lowered to a value at which albite crystals were expected, and held for >24 h. Charges were then quenched and analyzed using the methods as described above. In all cases, results of reversal experiments were consistent with the bracketing experiments.

Runs dealing with the change in melting temperature as a function of NaCl content were not reversed; however, generally similar run times as the pure H_2O runs and the more reactive NaCl-bearing system are assumed sufficient

for equilibrium conditions. In addition, the (Al, Si) order–disorder state of albite was determined for representative run products. Albite quenched from temperatures higher than 850 °C showed close approach to the high structural state $\left(\Delta 2\theta_{131-1\bar{3}1} \geq 1.9\right)$ in accordance with Goldsmith and Jenkins (1985a, b)

Solubility experiments employed run durations that were sufficient for equilibration in previous studies of the solubility of quartz in H_2O and H_2O–NaCl (e.g., Manning 1994; Newton and Manning 2000, 2008).

Liquidus and vapor-saturated solidus in the system $NaAlSi_3O_8$–H_2O

Results of experiments constraining the liquidus in the system $NaAlSi_3O_8$–H_2O at 1.0 GPa conducted between 700 and 1050 °C are given in Table 1 and Fig. 3. In experiments with insufficient H_2O for complete melting, albite coarsened substantially to form subhedral, rhomb-shaped crystals (Fig. 2a, c). Hydrous albite liquid in all experiments quenched to glasses that appear compositionally homogenous when observed by SEM using backscattered electrons. Quenched glasses from runs with more than about 8 wt% H_2O contained microscopically detectible bubbles (Fig. 2b). Bubble density and size in quenched glasses increased with bulk H_2O content. The absence of additional crystalline phases in run products confirmed congruent melting, which is consistent with previous studies.

The liquidus constraints from forward experiments were checked by reversal experiments at 800–900 °C and 8.00 ± 0.75 wt% H_2O, and 900–1050 °C and 7.25 ± 0.75 wt% H_2O. Runs Ab23, Ab234 and Ab236 indicated that final conditions were subliquidus, whereas crystal-free companion runs Ab235 and Ab237 indicated final conditions above the liquidus.

The H_2O-saturated solidus was constrained to lie between 690 and 700 °C. H_2O-rich experiments at 690 °C showed no evidence for melting (Table 2). In contrast, quenched melt was present in all experiments at 700 °C. Our criterion for vapor saturation at immediately supersolidus conditions is the presence of a void space in the quenched capsule with clear glassy spherules precipitated from a vapor phase (Fig. 2b). The solubility of H_2O at the minimum melting temperature of 695 ± 5 °C is 18.14 ± 1.35 wt% H_2O, as constrained by runs Ab9 (16.79 wt% H_2O) and Ab25 (19.48 wt% H_2O), in which run products show evidence for the presence of Ab + liquid and liquid + vapor at run conditions, respectively.

The results at 700–1050 °C indicate that at 1.0 GPa, the liquidus in the system $NaAlSi_3O_8$–H_2O displays shallow concave-up curvature (Fig. 3). The vapor-saturated and vapor-absent melting data were fitted to a third-order polynomial. We carried out three fits to the data set, in which the intercept of w_{H_2O} is fixed at reported dry melting temperatures of 1195 °C (Boettcher et al. 1982), 1217 °C (Birch and LeComte 1960), or 1235 °C (Boyd and England 1963). The best fit,

$$T = -2.0331 \times 10^{-3} w_{H_2O}^3 + 1.6497 w_{H_2O}^2 - 58.963 w_{H_2O} + 1235.5\ ^\circ\mathrm{C} \quad (1)$$

where T is in °C, and w_{H_2O} is H_2O concentration in wt%, was obtained using the Boyd and England (1963) melting

Table 1 Experimental results in the system $NaAlSi_3O_8$–H_2O at 1.0 GPa

Run	T (°C)	Time (h)	H_2O (wt %)	Result
Ab9	700	68	16.79	$L + Ab$
Ab24	700	64	18.02	L
Ab25	700	64	19.48	$L + V$
Ab231	700	93	22.55	$L + V$
Ab5	750	24	10.93	$L + Ab$
Ab8	750	22	11.72	$L + Ab$
Ab6	750	19	12.56	L
Ab2	800	50	4.06	$L + Ab$
*Ab23	900	22	8.01	(L)
	800	46		$L + Ab$
Ab1	800	50	8.79	$L + Ab$
Ab260	800	48	9.68	$L + Ab$
Ab7	800	24	10.11	$L + Ab$
Ab262	800	16	10.70	$L + Ab$
Ab4	800	24	11.40	L
Ab3	800	24	13.35	L
Ab27	800	68	26.13	$L + V$
Ab11	850	23	6.44	$L + Ab$
Ab15	850	24	7.23	$L + Ab$
*Ab236	900	15	7.24	(L)
	850	27		$L + Ab$
*Ab237	900	15	8.73	(L)
	850	27		L
*Ab234	1050	4	6.57	(L)
	900	42		$L + Ab$
Ab16	900	23	6.61	$L + Ab$
*Ab235	1050	4	7.95	(L)
	900	42		L
Ab79	950	67	4.99	$L + Ab$
Ab78	950	67	6.49	L
Ab258	1050	20	3.08	$L + Ab$
Ab259	1050	20	4.14	L

Errors in the H_2O content are in the fourth decimal place

Ab albite, *L* liquid, *V* vapor

* Reversal runs presented on two lines, the first indicating *T* and time where liquid can be assumed present, indicated by (*L*), and the second the final *T*, time and result

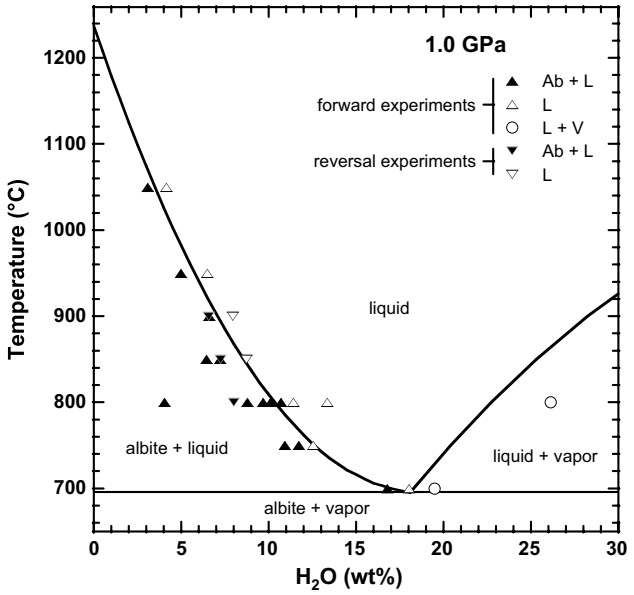

Fig. 3 Experimental results in the system $NaAlSi_3O_8$–H_2O at 1.0 GPa. *Triangles* indicate experiments constraining the liquidus curve. *Filled symbols* indicate albite +liquid; *open symbols*, liquid only. Forward and reversed experiments are indicated, respectively, with *upward* and *downward pointing triangles*. *Open circles* indicate coexisting liquid and vapor at run conditions. The liquidus curve was calculated from Eq. 1, and the liquid + vapor was calculated with derived Margules parameters (see text)

T and yielded the highest R^2 and a standard deviation (σ) of 0.85, slightly better than results based on Birch and LeComte ($\sigma = 0.90$) or Boettcher et al. 1982 ($\sigma = 1.13$).

Albite solubility in the system $NaAlSi_3O_8$–H_2O ± NaCl

Results of experiments on the solubility of crystalline albite in H_2O and H_2O + NaCl are given in Table 2 and Fig. 4. All experiments were conducted at 690 °C and 1.0 GPa. No additional stable crystalline phases were noted in any experiments, confirming congruent dissolution of albite. Albite solubility in H_2O at 690 °C was determined to be 8.79 ± 0.60 wt%. Albite solubility in H_2O–NaCl solutions initially decreases very strongly with addition of small amounts of NaCl (Fig. 4); at higher NaCl concentrations, the effect of progressively greater NaCl concentrations is more subdued. Extrapolation of Ab_1 results to zero mole percent NaCl yields agreement with Ab_2 experiments. The strong inhibition of albite dissolution in saline solutions is more pronounced than found in solubility studies of other minerals, including quartz at comparable temperatures (e.g., Newton and Manning 2010; Shmulovich et al. 2001). There is however a close resemblance to the near exponential drop-off in the solubility of quartz in saline solutions just below the melting temperature at higher pressures, 900–1100 °C and 1.5–2.0 GPa (Cruz and Manning 2015).

There were minute crystals (on the order of 1 μm) of a highly birefringent quench phase in the solubility measurements in pure H_2O. These were interpreted to be sodium mica or hydromica. Importantly, larger residual crystals that would signal incongruent dissolution (e.g., paragonite or corundum) were not observed in any of the experiments. Experiments with pure H_2O yielded strongly alkaline quench solutions of pH ≥ 12, implying that the

Table 2 Results of experiments on albite solubility in H_2O–NaCl and pure H_2O solutions at 1.0 GPa, 690 °C

Run	Type	Time (h)	H_2O (mg)	NaCl (mg)	NaCl (mol%)	Ab in (mg)	Ab out (mg)	Ab solubility (wt %)	Quench pH
Ab273	Ab_1	26	30.8334	0.5907	0.587	6.2510	3.3687	8.402 (34)	12
Ab267	Ab_1	81	24.9717	1.4852	1.800	2.3215	0.8013	5.434 (10)	10
Ab266	Ab_1	72	25.3026	4.4040	5.092	1.6343	0.7833	2.785 (4)	9
Ab268	Ab_1	92	25.2444	10.7787	11.631	1.8887	1.2497	1.743 (4)	7
Ab269	Ab_1	48	25.5106	23.4898	22.109	1.8621	1.4217	0.891 (1)	7
Ab274	Ab_1	96	24.7001	33.6767	29.592	1.4835	1.1796	0.518 (2)	7
Ab270	Ab_2	68	31.1201	–	–	3.8338	+Ab	<10.9682	11–12
Ab271	Ab_2	88	32.6197	–	–	4.6485	+Ab	<12.47313	12
Ab275	Ab_2	90	19.2869	–	–	1.9980	+Ab	<9.3869	12
Ab276	Ab_2	88	34.4563	–	–	3.0734	−Ab	>8.1892	12

Solubility reported in weight percent as $\frac{\Delta m_{Ab}}{\Delta m_{Ab}+m_{H_2O}+m_{NaCl}} \times 100$

Run types Ab_1, single-crystal weight loss experiments; Ab_2, saturated/undersaturated bracketing experiments (see text). Abbreviations *+Ab* albite remaining after experiment, *−Ab*, no albite remaining after experiment. NaCl mol% is reported for the initial solution and thus does not include dissolved albite

Uncertainties: average standard error in weighings is 0.4 μg; errors propagated to Ab solubility are given in parentheses

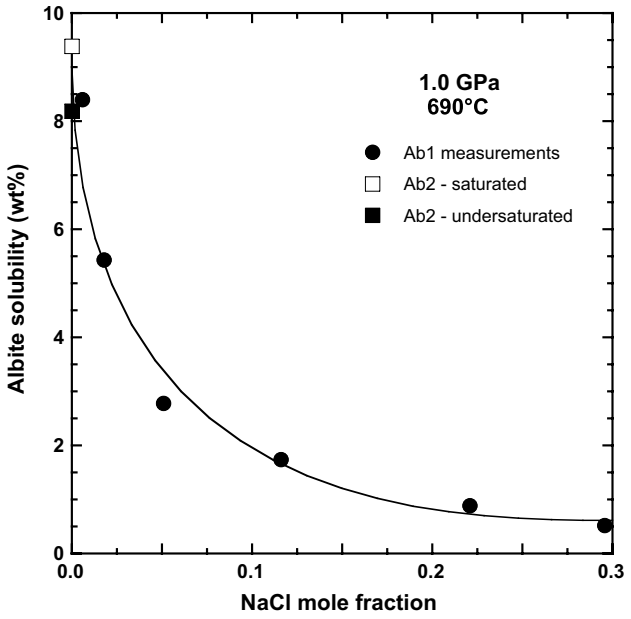

Fig. 4 Albite solubility determinations in pure H_2O (*squares*) and H_2O–NaCl solutions (*circles*) at 1.0 GPa and 690 °C. Results show that addition of NaCl strongly inhibits the albite dissolution in NaCl-rich brines. The *curve* was hand-drawn into fit the data. The midpoint of the Ab_2 experiments (see text) yields albite solubility of 8.79 ± 0.60 wt% in NaCl-free H_2O. Compositions calculated relative to the bulk fluid composition (H_2O, NaCl and dissolved solutes; Table 2). All experiments were conducted at halite-undersaturated conditions

quenched glass contains slight excesses of Al and Si, leaving the residual quench solutions NaOH-rich. Quench pH decreases markedly with increasing NaCl mole fraction, with near-neutral quench solutions produced from high-NaCl runs. The lower solubility of albite at high X_{NaCl} evidently limits the generation of alkaline quench solutions.

Liquidus in the system $NaAlSi_3O_8$–H_2O–NaCl

Results of experiments determining H_2O activity at the liquidus are given in Table 3 and Fig. 5a, b. Petrographic observation of run products confirmed congruent melting in the system albite–H_2O–NaCl. Selected quenched glasses from high-NaCl experiments were analyzed by EMP and found to contain 0.73–0.95 wt% Cl (Table 3), indicating low Cl solubility in the liquid. All runs contained large mass (47–81 %) of H_2O–NaCl fluid relative to albite to ensure vapor saturation (Table 3). A high fluid-rock ratio also has the advantage that the expected mass of H_2O dissolved in albitic liquids (based on the albite–H_2O experiments) represents a small fraction of the H_2O added to each run. This, combined with low Cl solubility in the melt, means that the starting H_2O and NaCl masses accurately reflect the fluid composition during an experiment. All experimental fluids had NaCl concentrations lower than that required for halite saturation at the T of interest (Aranovich and Newton 1996).

In general, run times were sufficient to yield complete melting to L + V. However, runs Ab247 and Ab252 at 950 and 1000 °C (Table 3) contained albite crystals and glass in the quenched charges. The crystal-rich portions showed vapor pockets containing halite crystals and glassy material (Fig. 2a). Because Cl solubility in the liquid is low, these are interpreted to reflect pockets of H_2O–NaCl vapor present during the experiment, from which halite crystallized upon quenching. As a test of this interpretation, a longer run was conducted at 950 °C (Ab250, 76 h), in which complete melting was observed. It was therefore assumed that runs Ab247 and Ab252 reflect supraliquidus conditions.

The structural state of run-product albite was determined by XRD. Runs Ab243 (850 °C), Ab239 (900 °C) and Ab256 (1050 °C) yielded $\Delta 2\theta_{131-1\bar{3}1}$ values of 1.909°, 1.936° and 1.952°, respectively, indicating close approach to high albite from the initially low structural state of the starting albite (Goldsmith and Jenkins 1985a, b).

Figure 5a shows the temperatures of our liquidus determinations as a function of H_2O mole fraction in mixed H_2O–NaCl fluids (Table 3). The data show that the temperature of vapor-saturated melting increases with decreasing H_2O mole fraction in the coexisting fluid phase. In view of the slightly sigmoid dependence on H_2O mole fraction, the data were fitted to a third-order polynomial with the intercept at $X_{H_2O} = 0$ fixed at the dry melting temperature of Boyd and England (1963):

$$T = -826.52X_{H_2O}^3 + 1358.0X_{H_2O}^2 - 1116.7X_{H_2O} + 1235.5\ ^\circ C \quad (2)$$

where T is in °C, X_{H_2O} is H_2O concentration in mole fraction, and $R^2 = 0.997$. Projection to dry albite melting is based on the expectation from low-pressure experiments relevant to the $NaAlSi_3O_8$–NaCl join (Kooster van Groos and Wyllie 1969), which suggest minimal melting point depression and a very albite-rich eutectic composition. This is supported by low NaCl contents of melts even at the most saline run conditions investigated yielding (<1 wt%; Table 3).

The low solubility of albite in H_2O–NaCl (Fig. 4) and the low NaCl content of the hydrous albite liquids allow calculation of a_{H_2O} from the activity formulation of Aranovich and Newton (1996). Figure 5b shows the variation in the temperature of the vapor-saturated liquidus as a function of H_2O activity in the liquid ($a^L_{H_2O}$) determined by controlling the H_2O activity in H_2O–NaCl fluids ($a^V_{H_2O}$) in equilibrium with hydrous silicate melt or albite. Results were extrapolated to the dry melting T of Boyd and England (1963) and vapor-saturated melting in the NaCl-free

Table 3 Experimental constraints on liquidus relations in the system $NaAlSi_3O_8$–H_2O–NaCl system at 1.0 GPa

Run	T (°C)	Time (h)	NaCl (mg)	H_2O (mg)	Ab (mg)	$X_{H_2O,i}$	$X_{H_2O,f}$	α	a_{H_2O}	Cl in glass (wt %)	Result
Ab245	800	13	19.3606	19.9008	19.7416	0.7693		1.0045	0.625		Ab + *V*
Ab249	800	139	10.6104	13.2025	10.8665	0.8015	0.7994	1.0045	0.665	nd	*L* + *V*
Ab246	800	50	9.5000	15.5376	10.1407	0.8414	0.8362	1.0045	0.718	nd	*L* + *V*
Ab241	850	90	20.1690	7.2503	20.5034	0.5384		0.8985	0.381		Ab + *V*
Ab242	850	14	20.1754	9.0180	20.5872	0.5918		0.8985	0.433		Ab + *V*
Ab243	850	71	20.4180	11.1416	18.9103	0.6390		0.8985	0.483		Ab + *V*
Ab244	850	95	21.0968	14.4060	22.4506	0.6890	0.6745	0.8985	0.522	nd	*L* + *V*
Ab239	900	68	15.4205	4.4385	21.8223	0.4829		0.7917	0.343		Ab + *V*
Ab240	900	69	19.8116	6.4050	20.4992	0.5119		0.7917	0.369		Ab + *V*
Ab238	900	16	19.9047	9.2402	20.4926	0.6010	0.5462	0.7917	0.402	0.73	*L* + *V*
Ab248	950	23	21.3362	3.8765	20.8414	0.3708		0.6851	0.259		Ab + *V*
Ab250	950	76	20.0090	4.9180	6.9077	0.4436	0.4316	0.6851	0.311	0.82	*L* + *V*
Ab247	950	18	18.8232	4.6488	19.8369	0.4448	0.4160	0.6851	0.297	nd	Ab + *V* + *L*
Ab253	1000	16	19.5295	2.3182	7.8092	0.2780		0.5877	0.195		Ab + *V*
Ab252	1000	19	19.9035	3.6788	11.6965	0.3749	–	0.5877	0.274	nd	Ab + *V* + *L*
Ab256	1050	3.3	26.6625	1.6299	11.3303	0.1655		0.4994	0.117		Ab + *V*
Ab297	1050	16	24.3755	1.5369	11.8917	0.1698		0.4994	0.120		Ab + *V*
Ab254	1050	45	25.5988	2.4034	6.5103	0.2335	–	0.4994	0.169	0.95	*L* + *V*
Ab255	1050	5	26.1134	3.1345	9.5143	0.2803	0.2647	0.4994	0.194	0.87	*L* + *V*

Ab albite, *L* melt, *V* aqueous fluid; $X_{H_2O,i}$ initial H_2O mole fraction added to capsule; $X_{H_2O,f}$ H_2O mole fraction in the vapor after correction for H_2O dissolved in *L* (see text). with the hydrous melt ("–" where value could not be determined due to fracturing of quench glass); α association parameter (Aranovich and Newton 1996); a_{H_2O}, H_2O activity; *nd* not determined. Values of a_{H_2O} calculated following Aranovich and Newton (1996) using H_2O density from Holland and Powell (1991) and neglecting dissolved albite in the fluid. Propagated weighing uncertainties yield an average standard error in activity of 0.007. All experiments were below halite saturation at run conditions. See text for EMP methods

system (see "Implications for albite-H2O mixing" section). Activities are on a 1-oxygen basis (i.e., a mixing unit of $Na_{1/8}Al_{1/8}Si_{3/8}O$; Stolper 1982). A best fit yields

$$T = -469.16 a_{H_2O}^{L\,\frac{1}{2}} - 93.382 a_{H_2O}^{L} + 1235.5\,^{\circ}C \quad (3)$$

where T is in °C and $R^2 = 0.996$.

Discussion

The system $NaAlSi_3O_8$–H_2O

H_2O-saturated melting

Our results indicate that the temperature of H_2O-saturated melting is 695 ± 5 °C at 1.0 GPa. This broadly agrees with previous studies at or near this pressure, though subtle differences bear comment. Burnham and Jahns (1962), Luth et al. (1964), Boettcher and Wyllie (1969) and Bohlen et al. (1982) report wet melting temperature of <690, 692.5 ± 12.5, 685 ± 5, and 675 ± 5 °C, respectively. (The Luth et al. (1964) bracket reflects later reinterpretation by Luth (1976).) Though similar, these melting temperatures are consistently slightly lower than our value. However, all four studies employed synthetic albite crystallized from gels and relatively short-run durations. Boettcher and Wyllie (1969) found that their run-product albite was in the high structural state. The albite state of order is not reported in the other works, but use of the same starting materials and similar or shorter run durations suggests that these studies determined H_2O-saturated melting of high albite. In contrast, our result reflects H_2O-saturated melting of low albite, as confirmed by XRD analysis of the starting material. Goldsmith and Jenkins (1985a, b) report the melting of low albite at 700 °C and 1.1 GPa, assuming the "rare quench glass" in their run products indicates melting. They show that, at the same P, high albite + H_2O yields liquid at 685 ± 5 °C. Thus, the lower melting temperature of high albite likely explains the small discrepancy between our new result and earlier work. Stalder et al. (2000) reported wet melting at 1.0 GPa at about 15–20 °C higher than Goldsmith and Jenkins (1985a, b) using low albite as a starting material, but they ascribe this discrepancy to the presence of minor CO_2 in their charges. Notably, thermodynamic models (e.g., Silver and Stolper 1985, 1989; Zeng and Nekvasil 1996; Holland and Powell 2001) yield vapor-saturated melting temperature ≤690 °C at 1.0 GPa.

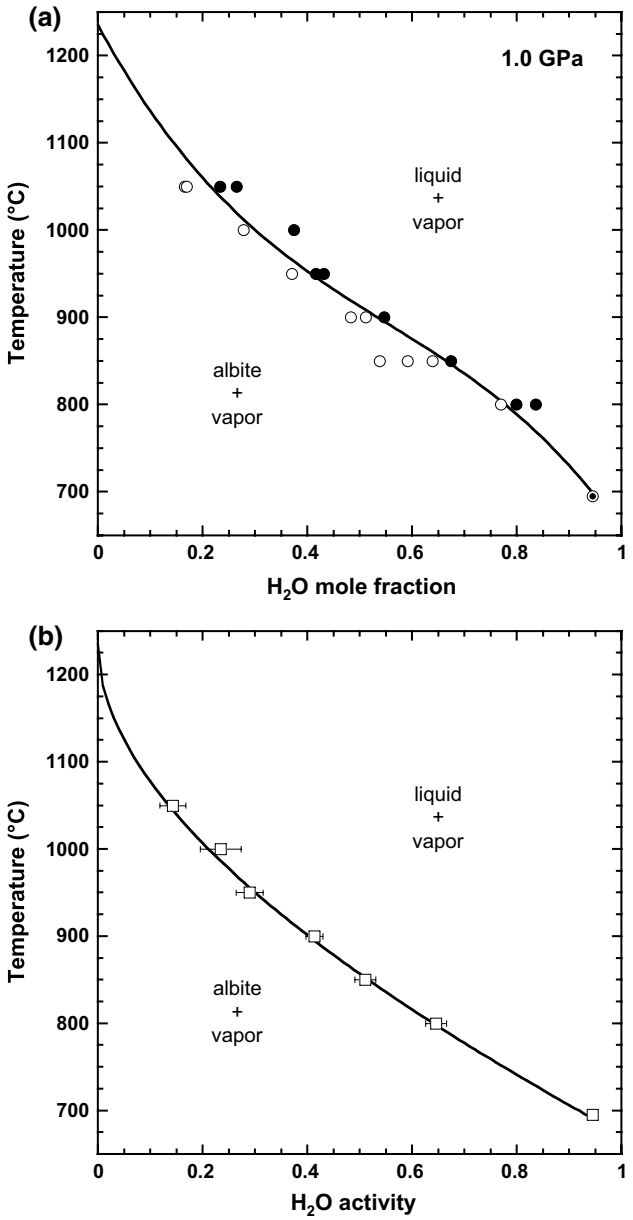

Fig. 5 Experimental results on the liquidus in the system $NaAlSi_3O_8$–H_2O–NaCl at 1.0 GPa and 695–1050 °C. **a** Results as a function of H_2O mole fraction. *Open circles* indicate no melt present; *filled circles*, melt present (Table 3). With the exception of NaCl-free melting at H_2O saturation (*dotted circle*), the composition of the fluid phase neglects minor dissolved albite but takes into account H_2O dissolved into the melt as determined by mass balance (Table 3). The fluid composition at NaCl-free vapor-saturated melting at 695 °C (*dotted circle*) is $X_{H_2O} = 0.945$; dissolved albite (calculated on a 1-oxygen basis; see text) is included because of its substantially higher solubility in pure H_2O (Fig. 4). The liquidus curve, derived using Eq. 2, is forced through the dry melting temperature of Boyd and England (1963), as justified by the high melting temperature at low X_{H_2O} and low solubility of Cl in the melt (see text). **b** Results as a function of H_2O activity (Aranovich and Newton 1996), shown as *midpoints* between the most constraining experiments in **a**. Uncertainties in the activity determinations reflect bracket widths. As in **a**, fluid compositions neglect dissolved albite except for the result at H_2O-saturated melting in the NaCl-free system, where $a_{H_2O} = X_{H_2O} = 0.945$. The liquidus curve was derived using Eq. 3

We find that the solubility of H_2O in H_2O-saturated albite liquid is 18.14 ± 1.35 wt% H_2O. This agrees within error with previous 1.0 GPa determinations of 16.9 ± 0.3 wt% (Burnham and Jahns 1962) and 18 wt% (Khitarov and Kadik 1973), which are the only previous determinations at this *P*.

Our data indicate that the solubility of albite in H_2O at the vapor-saturated solidus is 8.79 ± 0.60 wt% and that albite dissolves congruently at this *T*. The solubility is similar, but lower than the value of 10.20 wt% at 0.97 GPa and 700 °C derived by Burnham (in Clark 1966), as well as the value plotted in Fig. 1a of Khitarov and Kadik (1973). Zeng and Nekvasil (1996) provide an equation for albite solubility based on unpublished data of Paillat and Brown; however, at 690 °C and 1.0 GPa the predicted solubility of 21.15 wt% is more than a factor of two higher than our measured value, likely due to extrapolation of their model beyond conditions over which it is calibrated. Previous studies of albite solubility in H_2O near 1.0 GPa and $T \leq 650$ °C demonstrated incongruent dissolution in pure H_2O (Anderson and Burnham 1983; Shmulovich et al. 2001; Antignano and Manning 2008). Stalder et al. (2000) found that at 665–720 °C and 1.0 GPa, solute stoichiometry differed from that of albite, indicating incongruent dissolution. However, their fluids were interpreted to contain CO_2, which is likely to modify strongly the solute stoichiometry and concentration, even at low concentration. Our finding of congruent albite dissolution about 5 °C below the solidus implies that albite stoichiometry is approached in a narrow *T* interval just below the solidus. This is consistent with similar results of Stalder et al. (2000) at higher *P* of 1.7 GPa (T = 625–690 °C) and is required by previous studies locating the vapor-saturated solidus, which point to congruent melting.

Liquidus and dry melting temperature

There are numerous depictions and models of the albite–H_2O liquidus surface at 1.0 GPa; however, H_2O-undersaturated melting has not previously been investigated experimentally at this pressure. The experiments constrain a concave-up curvature of the liquidus (Fig. 3), which contrasts with the curvature at low pressure and with 1.0 GPa topologies shown by Khitarov and Kadik (1973) and Paillat et al. (1992) which instead show concave-down curvature. However, it is consistent with thermodynamic models (e.g., Holland and Powell 2001). Concave-up curvature is the expected topology for a system displaying closure of the L + V miscibility gap at intermediate compositions (e.g., Hack et al. 2007), as is predicted at 1.0 GPa for albite–H_2O (Shen and Keppler 1997; Hayden and Manning 2011).

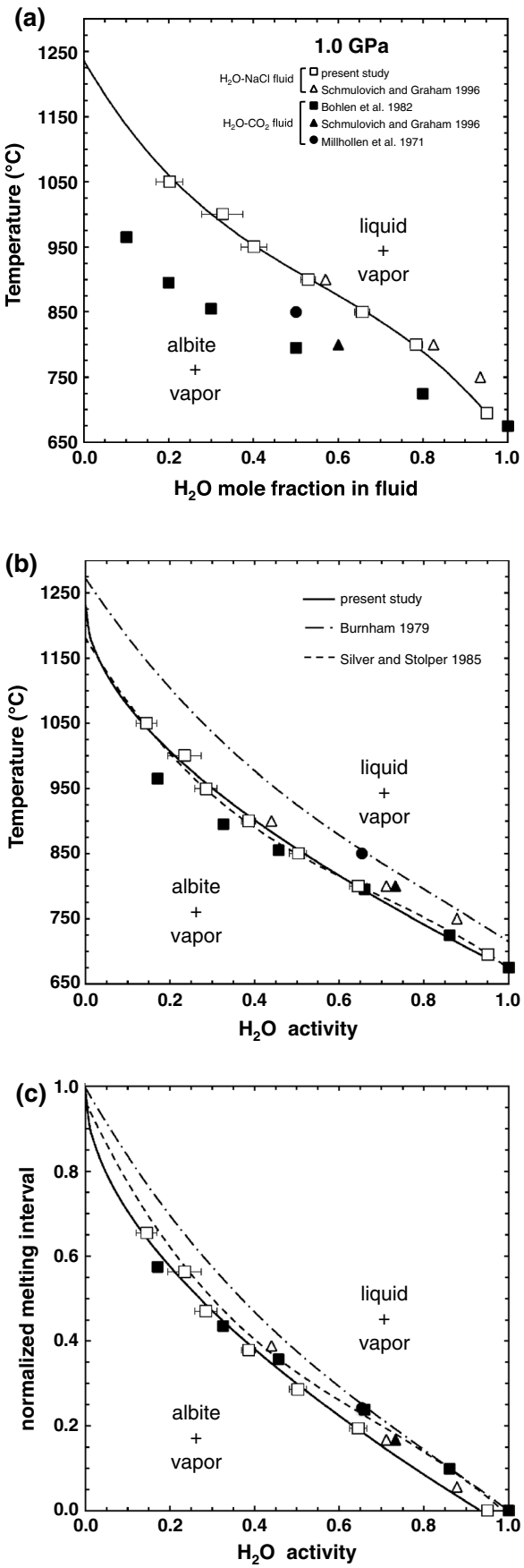

Fig. 6 Comparison of liquidus determinations with those in previous investigations in the systems $NaAlSi_3O_8$–H_2O–NaCl and $NaAlSi_3O_8$–H_2O–CO_2 at 1.0 GPa. **a.** Results as a function H_2O mole fraction. Fluid composition calculated as in Fig. 5. *Open symbols*, results in H_2O–NaCl fluids; *filled symbols*, H_2O–CO_2 fluids. The data of Shmulovich and Graham (1996) were obtained at 0.92 GPa. The *lower line* is hand-drawn through the data of Bohlen et al. (1982). **b** Results as a function H_2O activity in the liquid. All data are converted to H_2O activity using the formulations of Aranovich and Newton (1996;1999).The *lines* represent liquidus temperature as a function of water activity in the melt from Burnham (1979), Silver and Stolper (1985), and the present study. *Symbols* as in **a**. **c.** Results as a function H_2O activity in the liquid, with T normalized to the melting interval used in each study. The melting interval ranges from 0 to 1 and is defined as the difference between observed T and the H_2O saturated melting T, divided by the dry melting T minus the H_2O saturated melting T. *Lines* and *symbols* as in **a** and **b**

Albite solubility and melting in the presence of mixed fluids

H_2O–NaCl fluids

There are no previous measurements of albite solubility in H_2O–NaCl fluids at 1.0 GPa. Shmulovich et al. (2001) determined albite solubility in H_2O–NaCl at 0.9 GPa and 500–650 °C, but they likely encountered a field of stable paragonite at these low temperatures in pure H_2O (Wohlers et al. 2011). Nevertheless, the strong decrease in albite solubility with NaCl content of the fluid at 690 °C that we observe is similar to that seen by Shmulovich et al. (2001) at 0.9 GPa and 650 °C (Fig. 6b).

Shmulovich et al. (2001) investigated the change in liquidus temperature at saturation with H_2O–NaCl fluids at 0.9 GPa and 650 °C, though over a more limited range of H_2O-rich compositions. Their results are compared with our determinations in Fig. 6a, b, where it can be seen that agreement is quite good despite the small pressure difference. In particular, our data describe a slightly sigmoidal dependence of liquidus temperature on H_2O mole fraction.

Comparison to H_2O–CO_2 fluids

Albite melting at 1.0 GPa has also been investigated in the presence of H_2O–CO_2 fluid (Millhollen et al. 1971; Bohlen et al. 1982; Shmulovich and Graham 1996). Results for CO_2-bearing fluids are compared with those for NaCl-bearing fluids in Fig. 6a. The data confirm that there are large differences in the compositional dependence of the liquidus temperature when melt coexists with H_2O–NaCl versus H_2O–CO_2 fluids, as noted by Shmulovich and Graham (1996).

Because NaCl and CO_2 solubilities are low in hydrous albite liquid (Eggler and Kadik 1979; this study), and albite solubility is low in the two H_2O bearing fluids (Shmulovich et al. 2001; this study), the difference between the liquidi in Fig. 6a results directly from the different mixing

properties of the two binary fluid systems (Manning and Aranovich 2014): Deviations from ideality are negative in the H_2O–NaCl system (Aranovich and Newton 1996), but concave-up in the H_2O–CO_2 system (Aranovich and Newton 1999). Moreover, because the melt may be considered a binary $NaAlSi_3O_8$–H_2O mixture regardless of the coexisting mixed fluid (H_2O–CO_2 or H_2O–NaCl), the liquidus surface should be similar when portrayed as a function of H_2O activity in the liquid.

Figure 6b compares liquidi in the presence of H_2O–NaCl and H_2O–CO_2 fluids. For consistency and improved accuracy, the updated activity models of Aranovich and Newton (1996, 1999) were applied to the results of this study and those of Millhollen et al. (1971), Bohlen et al. (1982), and Shmulovich and Graham (1996; data at 0.9 GPa). At lower temperatures and higher H_2O concentrations, the agreement with the present data based on the activity of H_2O in NaCl solutions is very good. At lower H_2O concentrations and higher temperatures, the calculated liquidus H_2O activity points deviate negatively from the present values. The H_2O activity values shown by Silver and Stolper (1985) in their Fig. 2 are also in good agreement with the present measurements, though their activity-concentration function differs from ours. When the temperatures are scaled (Fig. 6c) according to the different dry melting temperatures of albite $\left(T_w^{\circ}\right)$ and the solidus temperatures (T_w) adopted by Millhollen et al. (1971), Bohlen et al. (1982), Shmulovich and Graham (1996) and this study, all data sets largely agree within error in the range of geologically relevant temperatures where granite genesis dominantly occurs.

Figure 6b, c shows that the liquidus H_2O activity function at 1.0 GPa calculated by Burnham (1979) differs considerably from the present measurements. Using our H_2O concentration in albitic liquid measurements, the activity coefficient γ_{H_2O} $\left(a_{H_2O}/X_{H_2O}\right)$ is smaller than his estimate by a factor of nearly two at 1050 °C. In contrast, the model of Silver and Stolper (1985) agrees well with the present results.

Our results show that primary control on the albite liquidus temperature is the H_2O activity, irrespective of whether the fluid in equilibrium with the melt is composed of H_2O–CO_2, or H_2O–NaCl. This relationship was found to be true for the liquidus in the haplogranite system by Aranovich et al. (2013). This implies that our results can be used as a guide for melting in the presence of more complex fluids.

Implications for $NaAlSi_3O_8$–H_2O mixing

Our constraints on the compositions of H_2O-saturated albite liquid and albite-saturated vapor at the wet solidus (Fig. 1, compositions at Points B and D) allow derivation of the thermodynamic properties of liquid–vapor mixing in the albite–H_2O binary. The system may be characterized using a subregular solution model, involving albite on a 1-oxygen basis (i.e., a mixing unit of $Na_{1/8}Al_{1/8}Si_{3/8}O$) and H_2O. The Margules mixing parameters W_{Ab} and W_{H_2O} may be determined by setting the activities of H_2O and $NaAlSi_3O_8$ equal in coexisting liquid and vapor

$$a^L_{H_2O} = a^V_{H_2O}, \tag{4}$$

$$a^L_{Ab} = a^V_{Ab}, \tag{5}$$

where the activity of each component in a phase (ϕ) (i.e., the liquid or the vapor) is given by

$$\ln a^{\phi}_{H_2O} = \ln X^{\phi}_{H_2O} + {X^{\phi}_{Ab}}^2\left[W_{H_2O} + 2X^{\phi}_{H_2O}\left(W_{Ab} - W_{H_2O}\right)\right]/RT, \tag{6}$$

$$\ln a^{\phi}_{Ab} = \ln X^{\phi}_{Ab} + {X^{\phi}_{H_2O}}^2\left[W_{Ab} + 2X^{\phi}_{Ab}\left(W_{H_2O} - W_{Ab}\right)\right]/RT. \tag{7}$$

The factor W_{Ab} in Eqs. 6 and 7 is the excess partial molar free energy change when 1/8 mol of $NaAlSi_3O_8$ liquid is mixed with a large amount of H_2O at fixed temperature and pressure. The two compositions input into this formulation are the albite solubility measurement in pure H_2O of 8.79 ± 0.60 wt% at 690 °C and the vapor-saturated solidus composition of 18.14 ± 1.35 wt% H_2O. Use of these values, in combination with Eqs. 4–7, yields Margules mixing parameters of $W_{H_2O} = 10.50 \pm 0.74$ kJ/mol and $W_{Ab} = 25.56 \pm 0.54$ kJ/mol and in turn a value of $a^L_{H_2O} = a^V_{H_2O} = 0.962 \pm 0.003$ at the solidus. This compares favorably with the value of 0.945 derived from experiments by assuming that $X^V_{H_2O} = a^V_{H_2O}$.

The value of $a^L_{H_2O} = a^V_{H_2O} = 0.962 \pm 0.003$ at the solidus provides an anchor at NaCl-free conditions for the determination of the H_2O activity along the liquidus from melting relations in H_2O–NaCl fluids. In addition, accounting for the solubility of albite in H_2O has important implications for the topology of the albite–H_2O binary: nonzero solubility is an essential feature in a system exhibiting relatively low temperature closure of the $L + V$ miscibility gap (Fig. 1). Although early studies recognized that the solubility of albite in H_2O was finite (Burnham in Clark 1966), with the exception of Blencoe (1992) and Zeng and Nekvasil (1996), the effect has largely been ignored, presumably due to a focus primarily on phase relations in the low-H_2O part of the binary.

The magnitude of the free energy change can be compared to that in other SiO_2-rich melts. Burnham and colleagues (Burnham and Davis 1974; Burnham 1975, 1979) advanced the conceptual model that melts of quartz and feldspars may be, from an energetic standpoint, considered quasi-crystalline substances. The high viscosity of the anhydrous liquids suggests that the strong Si–O bonding of the framework structure crystals is still mostly intact. Melting involves mainly loss of long-range order,

which requires substantially less energy input than disruption of Si–O linkages. Thus, $NaAlSi_3O_8$ liquids can, to a first approximation, be regarded as similar to a silica melt (Si_4O_8), on the bases of analogous crystal structures of albite and quartz, and similar responses of the liquids to dissolved H_2O. Extending this analogy to dissolution behavior near the vapor-saturated solidus, if Si_4O_8 is taken as a proxy for $NaAlSi_3O_8$ and if quartz represents liquid silica, then the Gibbs free energy of the equilibrium

$$\underset{\text{Quartz}}{SiO_2} + 2H_2O = \underset{\text{Solute}}{Si(OH)_4} \tag{8}$$

may be used as a comparison to W_{Ab}. Newton and Manning (2002, 2003) found that, at 1.0 GPa,

$$\Delta G_8^\circ = 66.84 - \frac{1.689 \times 10^4}{T} - \frac{6.520 \times 10^6}{T^2}, \tag{9}$$

where ΔG_8° is in kJ per mole, and T is in Kelvin. At 900 °C, $\Delta G_8^\circ = 47.7$ kJ/mol of SiO_2 converted to $Si(OH)_4$, or 23.8 kJ per mole of oxygen in silica, which agrees reasonably well with 25.56 kJ for 1/8 mol of $NaAlSi_3O_8$ derived from the subregular model assuming that W_{Ab} has only small variation with temperature.

Utilization of W_{Ab} and W_{H_2O} to describe the binary should account for the variation in these parameters with temperature. Although the liquidus data could be used to assess this variation, accuracy is improved using additional constraints from experimental characterization of the $L + V$ loop (e.g., Makhluf et al. 2013).

Implications for H_2O speciation in albite liquids

The subregular mixing model makes no account for the speciation of H_2O in the liquid phase. Stolper (1982) showed that the primary species which must be considered are molecular H_2O and OH^-, and that their concentrations reflect the homogeneous equilibrium between three types of oxygen species in the melt

$$O^{2-} + H_2O = 2OH^-, \tag{10}$$

where O^{2-} represents energetically equivalent bridging oxygens. The equilibrium constant for Eq. 10 is

$$K_{10} = \frac{a_{OH^-}^2}{a_{H_2O} \times a_{o^{2-}}}. \tag{11}$$

If mixing is ideal (Stolper 1982; Silver and Stolper 1985;1989), $a_{o^{2-}}$ can be taken as a_{Ab}^L, the activity of 1/8 $NaAlSi_3O_8$ (Ab) in the melt. Using equations of Stolper (1982) and Silver and Stolper (1985) along with thermodynamic data for dry albite melting from Holland and Powell (2001) and our data on liquid composition along the liquidus (Eq. 1) leads to values for K_{10} and allows calculation of the mole fractions of the three H_2O species.

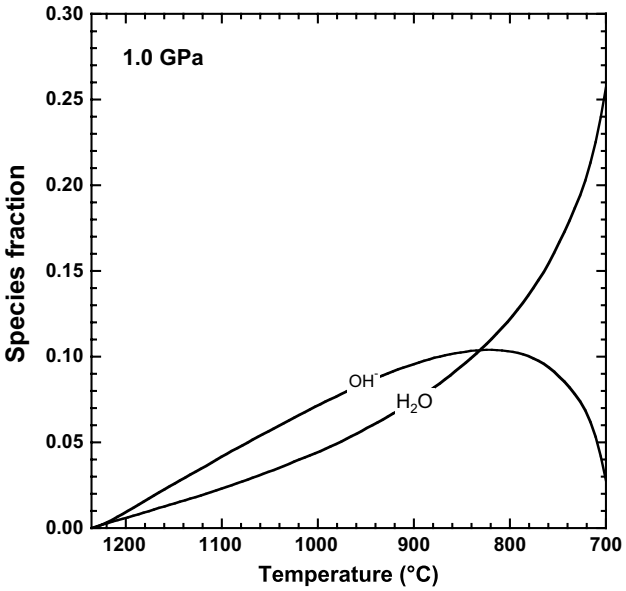

Fig. 7 Speciation of H_2O dissolved in hydrous albite liquids at 1 GPa, calculated using data Eq. 1 and the ideal solution model of Stolper (1982) and Silver and Stolper (1985). At high bulk H_2O concentrations and low temperatures approaching the vapor-saturated solidus, dissolved H_2O is dominated by molecular H_2O with only minor dissociation to OH^-

Figure 7 illustrates the variation in the distribution of H_2O and OH^- along the liquidus, calculated assuming ideal mixing (Stolper 1982; Silver and Stolper 1985, 1989). Our new liquidus constraints imply that, with increasing bulk H_2O content in the melt approaching the vapor-saturated solidus, dissolved OH^- initially predominates at low H_2O concentration (high T). However, as H_2O concentration increases with declining temperature, dissolved molecular H_2O becomes predominant and OH^- negligible near the solidus. This is broadly consistent with results at lower P (e.g., Silver and Stolper 1985, 1989), despite complications due to the potential non-quenchability of the H_2O speciation state (Nowak and Behrens 1995; Shen and Keppler 1995; Zhang 1999). Figure 7 shows that, given the modeling assumptions, as the H_2O-saturated solidus is approached, the concentration of OH^- tends rapidly toward zero and nearly all H_2O is present in molecular form. This is an important consideration for understanding the very high dissolved bulk H_2O, and the high H_2O activities (near unity), which must be obtained for critical mixing of L and V phases to occur (see below).

Implications for the $NaAlSi_3O_8$–H_2O phase diagram at 1.0 GPa

Burnham (1979) and Bohlen et al. (1982) experimentally derived activity-concentration estimates that did not yield critical mixing of albitic liquid and H_2O. The possibility

of this important aspect of the phase relations at elevated pressures was predicted by Paillat et al. (1992) based on improved measurement of the H_2O contents of glasses quenched from experiments in the binary system at pressures below 0.7 GPa. In contrast to previous workers, they found that at pressures above about 0.4 GPa, the solubility of H_2O in albite melts (vapor saturation) begins to increase with increasing temperature. Paillat et al. (1992) realized that this trend would lead to critical mixing of $NaAlSi_3O_8$ and H_2O at high pressures; that is, that the isobaric two-phase envelope between silicate melt (i.e., "liquid") and aqueous fluid (i.e., "vapor") will close to a critical point at some high temperature. They suggested a temperature of about 1250 °C at 1.0 GPa based on extrapolation of their data. The data of Shen and Keppler (1997) indicate a critical temperature near 1000 °C at 1.0 GPa, though pressure uncertainty is large. The results of Hayden and Manning (2011) and Kawamoto et al. (2012) suggested a slightly lower temperature (closer to 900 °C) of critical mixing at this pressure

The present data support critical mixing of the system $NaAlSi_3O_8$–H_2O at 1.0 GPa. The mixing parameters $W_{Ab} = 25.56\,kJ/mol$ and $W_{H_2O} = 10.50\,kJ/mol$ derived from our solidus composition measurements at 690 °C and 1.0 GPa should have only small temperature dependence, since the coexisting fluids are dense and have relatively small expansivity at high pressures. Assuming that W_{Ab} and W_{H_2O} are independent of temperature in the range 700-1100 °C, the two-phase envelope is predicted to close with increasing temperature to a critical point near 1100 °C and a critical composition of 55 wt% H_2O (Fig. 8a).

Figure 8b compares 1 GPa phase relations in the $NaAlSi_3O_8$-rich part of the binary, as determined in this study and in selected previous work (Silver and Stolper 1985; Zeng and Nekvasil 1996; Holland and Powell 2001). It can be seen that the new results indicate the highest H_2O solubility at the vapor-saturated solidus, consistent with direct experimental determinations (Burnham and Jahns 1962; Khitarov and Kadik 1973; this work). The decrease in liquidus T with H_2O at low H_2O contents is similar and would be more so if all used the same dry melting temperature of albite. Departures at higher H_2O contents result from different H_2O solubilities at minimum melting and different ways of treating K_{10}. The greatest difference is seen in the curve depicting the solubility of H_2O at vapor saturation. Nearly vertical slopes were obtained by Silver and Stolper (1985) and Holland and Powell (2001) because they assumed that (1) H_2O solubility in the liquid was independent of T and (2) H_2O activity in the vapor phase at the solidus was unity. As noted above, such models cannot yield critical mixing. Zeng and Nekvasil (1996) accounted for both factors, and their model yields critical mixing. Although 1 GPa is the extreme upper pressure limit of their model, it is nevertheless apparent that predicted liquidus topology, compositions at the solidus, solvus topology and critical temperature are inaccurate. It is evident that accurate account the nonzero solubility of $NaAlSi_3O_8$ in H_2O at the solidus temperature of 695 °C is necessary to model phase relations in the high-H_2O part of the binary.

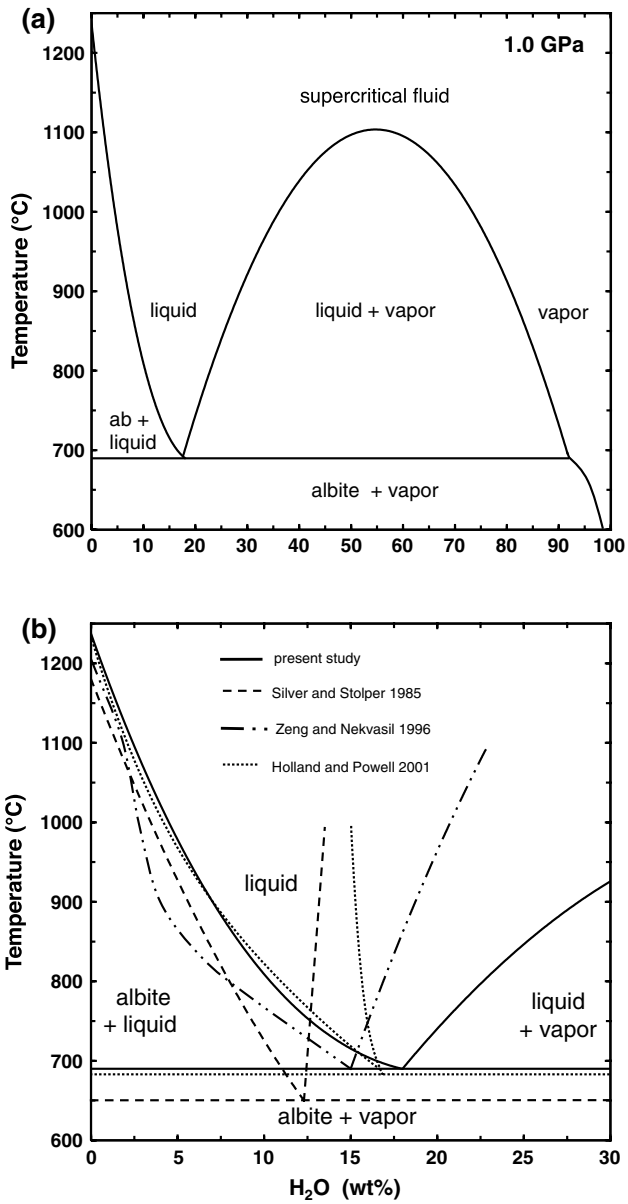

Fig. 8 **a** Quantitative $T - X_{H_2O}$ binary for the system $NaAlSi_3O_8$–H_2O at 1.0 GPa, as constrained by results of this study. Our results predict critical mixing at a temperature of about 1100 °C and composition of ~ 55 wt % H_2O. **b** Comparison of results of the present study with previous work, at relatively low bulk H_2O contents. Relative to previous estimates, our new experimental data imply higher temperature of melting at H_2O saturation, higher H_2O solubility at vapor-saturated melting and a shallow positive slop of the albite-rich limb of the L + V solvus

Application to petrology

The system $NaAlSi_3O_8$–H_2O is, by itself, limited in direct application to magmatic processes, though the principles it illustrates are very important to a thermodynamics-based understanding of granites. A more general application to petrology awaits expansion of the system to include quartz and K-feldspar. A reconnaissance study of a simple ternary granite by Bureau and Keppler (1999) showed that this more complex system also displays critical mixing of melt and aqueous fluid in much the same *P*–*T* range as for albite–H_2O. Further investigations involving solubility and H_2O activity measurements are therefore highly desirable.

Many features of granite petrology have been linked to high mineral solubility in the vapor phase at elevated *P* and *T*. These include such phenomena as ocellar, orbicular, graphic and rapakivi textures (Ballhaus et al. 2015). The assumption of essentially unit H_2O activity at deep-crustal pressures and temperatures adopted by numerous workers should give way to considerations of high solubility of mineral components in near-critical aqueous solutions. Aranovich et al. (2013) showed that H_2O activity measurements can be obtained for liquids in equilibrium with feldspars and quartz by melting experiments in the presence of (Na, K)Cl solutions. Extension of the present solubility and activity measurements to the simple granite–H_2O system would seem to be feasible in developing a thermodynamic theory of granitic magmatism.

Conclusions

1. Liquidus H_2O contents in the system $NaAlSi_3O_8$–H_2O were determined by reversed equilibration of a pure, natural albite at 1.0 GPa and 695–1050 °C. The liquidus has concave-up curvature, with rapid increase of H_2O content near the solidus temperature of 695 ± 5 °C. The solidus H_2O content of 18.14 ± 1.35 wt% agrees well with that of Burnham and Jahns (1962) using the same method of interpretation of the run products.
2. Solubility measurements on albite single crystals as well as on powdered albite confirm congruent solubility and a measurement of 8.79 ± 0.60 wt% albite in a pure H_2O solution at 690 °C and 1.0 GPa, which is just below the melting point of albite at that pressure. This non-negligible concentration of $NaAlSi_3O_8$ significantly affects the thermodynamic properties of the fluid. Critical phenomena would not be possible were it not for the appreciable solubility of albite in H_2O solution. The effect of NaCl on the solubility of albite is to greatly decrease the solubility of albite in H_2O rich vapor and of H_2O in albite-rich silicate liquid, and in turn, to increase the critical temperature to progressively higher temperatures not likely to be realized in typical geologic settings.
3. The low solubility of albite in H_2O–NaCl solutions makes possible a determination of the H_2O activity at the liquidus by equilibration of albite with concentrated NaCl solutions of known H_2O activity. The activity-concentration function along the liquidus, determined with NaCl solutions, is remarkably similar to that of Bohlen et al. (1982) when updated mixing properties of H_2O–CO_2 are used. This shows the power of formulating the liquidus temperature as a function of H_2O activity instead of simply H_2O concentration.
4. Using the H_2O speciation model of Stolper (1982) in combination with the current liquidus measurements determined here at 1.0 GPa as input show a substantial increase in molecular H_2O in the melt and a dramatic decline in OH^- near the vapor-saturated solidus. In contrast, OH^- is the dominant species at low bulk H_2O contents and high temperatures near the dry melting point of albite.
5. The fact that molecular H_2O is the dominant species at the onset of liquid–vapor immiscibility with a value of $a_{H_2O} = 0.962 \pm 0.003$ in the melt at the vapor-saturated solidus makes possible the subregular solution model with essentially a pure end-member solution of H_2O and $NaAlSi_3O_8$. As such, a Margules formulation of mixing of $NaAlSi_3O_8$–H_2O liquid and vapor is possible with only the input of the T-X_{H_2O} values at the vapor-saturated solidus and at the invariant point on the H_2O-rich limb of the solvus (determined by the solubility measurement). Margules parameters of 10.50 ± 0.74 and 25.56 ± 0.54 kJ/mol for H_2O and $NaAlSi_3O_8$ (on a one-oxygen basis), respectively, were obtained at these conditions, assuming no variation of the parameters with temperature. The solvus compositions at subcritical temperatures were calculated for the $NaAlSi_3O_8$–H_2O system with these mixing parameters. Critical phenomena are predicted at slightly higher temperatures than found by Shen and Keppler (1997; 1100 versus 1010 °C, respectively), but at the same critical composition of 55 wt% H_2O at 1.0 GPa. This method may provide a viable approach to investigating the topology of the solvus of $NaAlSi_3O_8$–H_2O at other pressures as well as in other mineral–H_2O systems that congruently dissolve at temperatures slightly below the solidus.

Acknowledgments We thank Professor Jacques Touret and Professor Leonya Aranovich for helpful discussions on this work, Rosario Esposito and Daniel Weidendorfer for assistance with EMP analysis and Saeed Khan for assistance with the XRD analysis. We are grateful to the reviewers D. Jenkins and L. Waters for their comments, which resulted in substantial improvements to the manuscript. This research was supported by NSF grant #EAR 1347987 to CEM.

References

Anderson GM, Burnham CW (1983) Feldspar solubility and the transport of aluminum under metamorphic conditions. Am J Sci 283(A):283–297

Antignano A, Manning CE (2008) Rutile solubility in H_2O, H_2O–SiO_2, and H_2O–$NaAlSi_3O_8$ fluids at 0.7–2.0 GPa and 700–1000 °C: implications for mobility of nominally insoluble elements. Chem Geol 255:283–293

Aranovich LY, Newton RC (1996) H_2O activity in concentrated NaCl solutions at high pressures and temperatures measured by the brucite–periclase equilibrium. Contrib Mineral Petrol 125:200–212

Aranovich LY, Newton RC (1999) Experimental determination of CO_2–H_2O activity-composition relations at 600–1000 °C and 6–14 kbar by reversed decarbonation and dehydration reactions. Am Mineral 84:1319–1332

Aranovich LY, Newton RC, Manning CE (2013) Brine-assisted anatexis: experimental melting in the system haplogranite–H_2O–NaCl–KCl at deep-crustal conditions. Earth Planet Sci Lett 374:111–120

Ballhaus C, Fonseca ROC, Münker C, Kirchenbaur M, Zirner A (2015) Spheroidal textures in igneous rocks—textural consequences of H_2O saturation in basaltic melts. Geochim Cosmochim Acta 167:241–252

Benusa MD, Angel RJ, Ross NL (2005) Compression of albite, $NaAlSi_3O_8$. Am Mineral 90:1115–1120

Birch AF, LeComte P (1960) Temperature–pressure plane for albite composition. Am J Sci 258:209–217

Blencoe JG (1992) A two-parameter Margules method for modelling the thermodynamic mixing properties of albite-water melts. Trans R Soc Edinb Earth Sci 83:423–428

Boettcher AL, Wyllie PJ (1969) Phase relations in the system $NaAlSiO_4$–SiO_2–H_2O to 35 kilobars pressure. Am J Sci 267:875–909

Boettcher AL, Burnham CW, Windom KE, Bohlen SR (1982) Liquids, glasses, and the melting of silicates to high pressures. J Geol 1:127–138

Bohlen SR, Boettcher AL, Wall VJ (1982) The system albite–H_2O–CO_2: a model for melting and activities of water at high pressures. Am Mineral 67:451–462

Boyd FR, England JL (1963) Effect of pressure on the melting of diopside, $CaMgSi_2O_6$, and albite, $NaAlSi_3O_8$, in the range up to 50 kilobars. J Geophys Res 68:311–323

Brown GC, Fyfe WS (1970) The production of granitic melts during ultrametamorphism. Contrib Mineral Petrol 28:310–318

Bureau H, Keppler H (1999) Complete miscibility between silicate melts and hydrous fluids in the upper mantle: experimental evidence and geochemical implications. Earth Planet Sci Lett 165:187–196

Burnham CW (1975) Water and magmas; a mixing model. Geochim Cosmochim Acta 39:1077–1084

Burnham CW (1979) The importance of volatile constituents. In: Yoder HS Jr (ed) The evolution of the igneous rocks: fiftieth anniversary perspectives. Princeton University Press, New Jersey, pp 439–482

Burnham CW, Davis NF (1974) The role of H_2O in silicate melts: II thermodynamic and phase relations in the system $NaAlSi_3O_8$–H_2O to 10 kilobars, 700°–1100 °C. Am J Sci 274:902–940

Burnham CW, Jahns RH (1962) A method for determining the solubility of water in silicate melts. Am J Sci 260:721–745

Clark SP (1966) Solubility. In: Clark SP (ed) Handbook of physical constants. The Geological Society of America Inc., New York, pp 415–436

Cruz MF, Manning CE (2015) Experimental determination of quartz solubility and melting in the system SiO_2–H_2O–NaCl at 15–20 kbar and 900–1100 °C: implications for silica polymerization and formation of supercritical fluids. Contrib Mineral Petrol 170:1–17

Eggler DH, Kadik AA (1979) The system $NaAlSi_3O_8$–H_2O–CO_2 to 20 kbar pressure: compositional and thermodynamic relations of liquids and vapors coexisting with albite. Am Mineral 64:1036–1048

Goldsmith JR, Jenkins DM (1985a) The high–low albite relations revealed by reversal of degree of order at high pressures. Am Mineral 70:911–923

Goldsmith JR, Jenkins DM (1985b) The hydrothermal melting of low and high albite. Am Mineral 70:924–933

Goranson RW (1938) Silicate-water systems: phase equilibria in the $NaAlSi_3O_8$—H_2O and $KAlSi_3O_8$—H_2O systems at high temperatures and pressures. Am J Sci 35:71–9l

Hack AC, Thompson AB, Aerts M (2007) Phase relations involving hydrous silicate melts, aqueous fluids, and minerals. Rev Mineral Geochem 65:129–185

Hayden LA, Manning CE (2011) Rutile solubility in supercritical $NaAlSi_3O_8$–H_2O fluids. Chem Geol 284:74–81

Holland TJ, Powell R (1991) A Compensated–Redlich–Kwong (CORK) equation for volumes and fugacities of CO_2 and H_2O in the range 1 bar to 50 kbar and 100–1600 °C. Contrib Mineral Petrol 109:265–273

Holland TJ, Powell R (2001) Calculation of phase relations involving haplogranitic melts using an internally consistent thermodynamic dataset. J Petrol 424:673–683

Kawamoto T, Kanzaki M, Mibe K, Matsukage KN, Ono S (2012) Separation of supercritical slab-fluids to form aqueous fluid and melt components in subduction zone magmatism. Proc Natl Acad Sci 109:18695–18700

Kennedy GC, Wasserburg GJ, Heard HC, Newton RC (1962) The upper three-phase region in the system SiO_2–H_2O. Am J Sci 260:501–521

Khitarov NI, Kadik AA (1973) Water and carbon dioxide in magmatic melts and peculiarities of the melting process. Contrib Mineral Petrol 41:205–215

Kooster van Groos AK, Wyllie PJ (1969) Melting relationships in the system $NaAlSi_3O_8$–NaCl–H_2O at one kilobar pressure, with petrological applications. J Geol 77:581–605

Krupka KM, Robie RA, Hemingway BS (1979) High-temperature heat capacities of corundum, periclase, anorthite, $CaAl_2Si_2O8$ glass, muscovite, pyrophyllite, $KAlSi_3O_8$ glass, grossular, and $NaAlSi_3O_8$ glass. Am Mineral 64:86–101

Lange RL, Carmichael ISE (1990) Thermodynamic properties of silicate liquids with emphasis on density, thermal expansion and compressibility. Rev Mineral Geochem 24:25–64

Luth WC (1976) Granitic rocks. In: Bailey DK, MacDonald R (eds) The evolution of the crystalline rocks. Academic Press, London, pp 335–417

Luth WC, Jahns RH, Tuttle OF (1964) The granite system at pressures of 4 to 10 kilobars. J Geophys Res 69:759–773

Makhluf AR, Newton RC, Manning CE (2013) New experimental constraints on liquidi, critical mixing, and the second critical end point in the system albite-H_2O. AGU Fall Meet Abstr 1:2624

Manning CE (1994) The solubility of quartz in H_2O in the lower crust and upper mantle. Geochim Cosmochim Acta 58:4831–4839

Manning CE, Aranovich LY (2014) Brines at high pressure and temperature: thermodynamic, petrologic and geochemical effects. Precambrian Res 253:6–16

Manning CE, Boettcher SL (1994) Rapid-quench hydrothermal experiments at mantle pressures and temperatures. Am Mineral 79:1153–1158

Millhollen GL, Wyllie PJ, Burnham CW (1971) Melting relations of $NaAlSi_3O_8$ to 30 kb in the presence of H_2O:CO_2 = 50:50 vapor. Am J Sci 271:473–480

Newton RC, Manning CE (2000) Quartz solubility in H_2O–NaCl and H_2O–CO_2 solutions at deep crust-upper mantle pressures and temperatures: 2–15 kbar and 500–900 °C. Geochim Cosmochim Acta 64(17):2993–3005

Newton RC, Manning CE (2002) Solubility of enstatite + forsterite in H_2O at deep crust/upper mantle conditions: 4 to 15 kbar and 700 to 900 °C. Geochim Cosmochim Acta 66:4165–4176

Newton RC, Manning CE (2003) Activity coefficient of aqueous silica at 800 °C, 12 kbar, from solubility measurements on SiO_2-buffering assemblages. Contrib Mineral Petrol 146:135–143

Newton RC, Manning CE (2008) Thermodynamics of SiO_2–H_2O fluids near the upper critical end point from quartz solubility measurements at 10 kbar. Earth Planet Sci Lett 274:241–249

Newton RC, Manning CE (2010) Role of saline fluids in deep-crustal and upper mantle metasomatism: insights from experimental studies. Geofluids 10:58–72

Newton RC, Smith JV (1967) Investigations concerning the breakdown of albite at depth in the earth. J Geol 1:268–286

Nowak M, Behrens H (1995) The speciation of water in haplogranitic glasses and melts determined by in situ near infrared spectroscopy. Geochim Cosmochim Acta 59:3445–3450

Paillat O, Elphick SC, Brown WL (1992) The solubility of water in $NaAlSi_3O_8$ melts: a re-examination of Ab–H_2O phase relationships and critical behaviour at high pressures. Contrib Mineral Petrol 112:490–500

Rutter MJ, Wyllie PJ (1988) Melting of vapour-absent tonalite at 10 kbar to simulate dehydration–melting in the deep crust. Nature 331:159–160

Shen A, Keppler H (1995) Infrared spectroscopy of hydrous silicate melts to 1000 °C and 10 kbar: direct observation of H_2O speciation in a diamond-anvil cell. Am Mineral 80:1335–1338

Shen A, Keppler H (1997) Direct observation of complete miscibility in the albite–H_2O system. Nature 385:710–712

Shmulovich KI, Graham CM (1996) Melting of albite and dehydration of brucite in H_2O–NaCl fluids to 9 kbars and 700–900 °C: implications for partial melting and water activities during high pressure metamorphism. Contrib Mineral Petrol 124:370–382

Shmulovich KI, Graham CM, Yardley BWD (2001) Quartz, albite and diopside solubilities in H_2O–NaCl and H_2O-CO_2 fluids at 05–09 GPa. Contrib Mineral Petrol 141:95–108

Silver LA, Stolper EM (1985) A thermodynamic model for hydrous silicate melts. J Geol 93:161–178

Silver L, Stolper E (1989) Water in albitic glasses. J Petrol 30:667–709

Stalder R, Ulmer P, Thompson AB, Günther D (2000) Experimental approach to constrain second critical end points in fluid/silicate systems: near-solidus fluids and melts in the system albite–H_2O. Am Mineral 85:68–77

Stebbins JF, Carmichael ISE, Moret LH (1984) Heat capacities and entropies of silicate liquids and glasses. Contrib Mineral Petrol 86:131–148

Stolper E (1982) The speciation of water in silicate melts. Geochim Cosmochim Acta 46:2609–2620

Tuttle OF, Bowen NL (1958) Origin of granite in the light of experimental studies in the system $NaAlSi_3O_8$–$KAlSi_3O_8$–SiO_2–H_2O. Geol Soc Am Memoirs 74:1–146

Tribaudino M, Angel RJ, Cámara F, Nestola F, Pasqual D, Margiolaki I (2010) Thermal expansion of plagioclase feldspars. Contrib Mineral Petrol 160:899–908

Wohlers A, Manning CE, Thompson AB (2011) Experimental investigation of the solubility of albite and jadeite in H_2O, with paragonite + quartz at 500 and 600 °C, and 1–2.25 GPa. Geochim Cosmochim Acta 75:2924–2939

Zeng Q, Nekvasil H (1996) An associated solution model for albite–water melts. Geochim Cosmochim Acta 60:59–73

Zhang Y (1999) H_2O in rhyolitic glasses and melts: measurement, speciation, solubility, and diffusion. Rev Geophys 37:493–516